XIII. INTERACTION OF LASER RADIATION WITH PLASMAS AND NONADIABATIC MOTION OF PARTICLES IN MAGNETIC FIELDS*

Academic and Research Staff

Prof. D. J. Rose
Prof. T. H. Dupree
Prof. L. M. Lidsky

Graduate Students

T. S. Brown
J. D. Callen
M. V. Cesarski
J. F. Clarke
D. E. Crane
J. N. Hamawi
W. T. Hebel
M. D. Lubin
R. W. Moir
A. A. Offenberger
M. A. Samis

A. INCOHERENT SCATTERING OF LIGHT FROM A PLASMA III

The adoption of an infrared laser, optics, and detector, for observation of cooperative scattering effects from a plasma, was previously reported.[1] Provided the signal-to-noise is not seriously degraded for detection of small signals in the infrared versus visible light, a great benefit in the form of enhanced spectral width is available, thereby enabling a more detailed experimental view of plasma cooperative effects. The attendent difficulties are mainly two: one being the considerable black-body radiation at a wavelength of 10 microns, the other arising because thermal wavelength detectors are not as sensitive as photomultipliers in visible light.

The H_2, CO_2 laser[2] was operated at an internal power level of several hundred watts, the measurement being achieved by coupling a fraction of the power out through a small hole in one mirror. A direct current discharge of ≈50 ma, at a field of 4 kv/meter in a gas mixture of 0.7 torr CO_2, 1.5 torr N_2, 2.8 torr He in a glass tube of 25 mm I.D. and 3 meters length yielded 1-watt cw coupled out through a 1-mm diameter hole in one mirror. Since the laser produces its power at a nominal 10.6 microns, NaCl windows and gold-coated mirrors (aligned in a hemispherical mode) formed the optical arrangement. Measurements were made with a calorimeter designed to measure power directly in the steady state. The power absorbed at one end of a copper rod gives a thermal conduction along the rod, which in a few heat-diffusion times relaxes to a constant energy conducted per unit time. The temperature difference between two points is linear with the input power, for nominal temperature rises; moreover, convective and radiative losses can be corrected for. It is anticipated that through a larger hole, a significant increase in power could be coupled out, and future work will explore this possibility.

With regard to the scattering experiment; the equivalent noise power, in the thermal fluctuations of dry-ice temperature black-body radiation, previously reported was

*This work was supported by the United States Atomic Energy Commission (Contract AT(30-1)-3285).

$P_N \approx 10^{-13}$ watt/(cps)$^{1/2}$. This calculation was based on an effective field of view of 6° for the mercury-doped germanium detector. In fact, to observe a larger scattering volume, a re-design has led to an F.O.V. ≈ 20°, thereby increasing noise. Furthermore, since it would be desirable to leave the optics at room temperature rather than to cool to dry-ice temperature, the more obvious way to proceed would be to use a cooled optical filter in front of the sensitive area of the detector. With the filter inside the cold shield of the detector (4°K), the filter would be essentially noise-free, the limiting noise being the background fluctuation level within the filter bandpass.

A comparison of the merits of cooling the background (temperature T_b) and reducing the bandwidth at the detector (nominal bandwidth ≈ 12 microns) is made in tabular form below. The detector has an area = 10^{-3} cm^2, and sees a solid angle $\Delta\Omega$ = 0.094 ster.

T_b(°K)	$\Delta\lambda(\mu)$	P_N(watts/(cps)$^{1/2}$)
300	12	4.3×10^{-13}
300	0.12	4.3×10^{-14}
195	12	1.3×10^{-13}
195	0.12	1.3×10^{-14}

Equally important with keeping noise power down to tolerable levels (since signal watts will be $\lesssim 10^{-14}$ watt) is the problem of achieving high enough detector responsivity = signal volts per unit power detected. The responsivity goes up proportional to the decrease in DC background radiation. Typically, a detector with full-wavelength bandwidth looking at a 300°K background has a responsivity of 4×10^5 volt watt^{-1}, whereas a reduction of 100 in DC background would give 4×10^7 volt watt^{-1}. At the former responsivity a signal voltage of only 2 nanovolts would have to be measured (from a source impedance of many hundred kilohms) which is considerably below the noise figure for any available preamplifier. Thus amplifier noise would intrude along with photon noise. Also, the photoconductive detector is quiescent current biased, and a load resistor couples out the signal. The Johnson noise of a 1-MΩ resistor is ≈130 nanovolts/(cps)$^{1/2}$ at room temperature, and ≈15 nanovolts/(cps)$^{1/2}$ at 4°K. Thus a high responsivity is mandatory, and the use of, or combination of, cooled optical filter and reduced background is required. The one disadvantage to reducing the background lies in the fact that the detector impedance goes up, typical values being ≈4 MΩ for a background noise power ≈10^{-13} watt/(cps)$^{1/2}$.

Noise measurements of several low-noise preamplifiers have been conducted, with noise source input impedances from a few hundred kilohms to 10 megohms. A preamplifier utilizing field-effect transistors with an input impedance of 1000 MΩ was tested, and

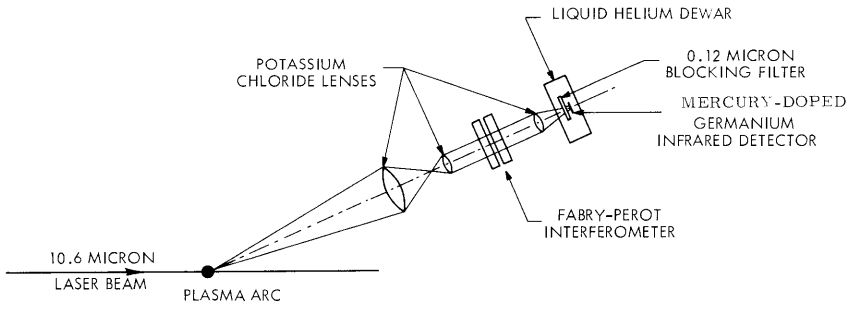

Fig. XIII-1. Experiment for observation of cooperative scattering effects from a plasma.

a high-Q bandpass filter for the output was designed and tested. The nominal noise voltage referred to the preamplifier input is 70 nanovolts/$(\text{cps})^{1/2}$ near 1 kc, with a source impedance of up to 10 MΩ. With the larger responsivity, then, the signal level will be equal to or greater than the amplifier noise.

The detector has provision for installing a narrow bandpass filter, and this will be done. The filter achieves two ends – namely, reducing the background fluctuation level, and blocking all of the lower and higher modes of the Fabry-Perot interference filter. An over-all schematic diagram of the experiment is shown in Fig. XIII-1. The question of whether the plasma will be intracavity to the laser, or whether a focused external beam will be used, will depend on the final ratio of internal to external watts.

A. A. Offenberger

References

1. A. A. Offenberger, Quarterly Progress Report No. 79, Research Laboratory of Electronics, M.I.T., October 15, 1965, p. 145.
2. C. K. N. Patel, Phys. Rev. Letters 13, 617 (1964).

B. NONADIABATIC TRAPPING IN TOROIDAL GEOMETRY

The construction of a toroidal nonadiabatic electron trap[1] is now complete, and a cw circulating electron beam has been achieved. This report describes measured and calculated characteristics of the injected and trapped electron beam.

The device consists of a racetrack-shaped torus, 6.15 meters long with an 11.1-cm I.D. The straight sections are 1.45 m long, B = 70 gauss, injection energy E = 2.0 kV, base pressure in the 10^{-6} torr range, Larmor radius (if all 2.0 kV are in the perpendicular direction) r_{b_o} = 2.1 cm. The U-bend drifts are cancelled by vertical magnetic fields. Rotational transform windings have been installed, but are not being used at present. The electron beam (a few microamperes) is injected at an angle of 63.3° with respect

to the magnetic field. This results in a Larmor radius r_b = 1.9 cm with 80% of the beam energy perpendicular to B.

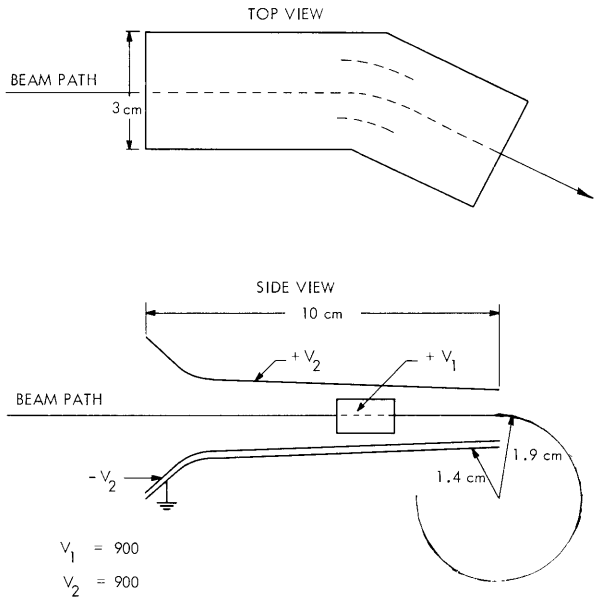

Fig. XIII-2. Electron-beam injector.

Figure XIII-2 shows the injector configuration. The injection point is one Larmor radius off-axis so that the guiding center is on the axis. The vertical electrostatic plates furnish the proper E field to yield a horizontal trajectory to the tip of the injector snout. A horizontal deflector bends the beam through an angle of 26.7° in the horizontal plane. The beam is thus injected as a helix of radius 1.9 cm and pitch 6.0 cm. The beam then encounters the "corkscrew"[2] which has been designed to transform perpendicular energy to parallel energy by resonant perturbation of the orbit. The corkscrew produces a small magnetic field (3.0 gauss) which is perpendicular to the main field and rotates in space with a pitch that increases with length (see Fig. XIII-3) in synchronism with the pitch of the beam. Thus the beam "sees" a $\vec{v} \times \vec{B}$ force which monotonically increases the parallel energy and straightens or "unwinds" the helical beam.

The performance of the corkscrew in unwinding the beam was checked by analyzing the parallel energy of the beam with a retarding potential screen and Faraday cup appropriately biased to retain secondary electrons. The parallel energy distribution is shown in Fig. XIII-4. Ideally the beam at the input to the corkscrew would be a spike at 400 volts, and the output a spike at 2000 volts. In reality the input beam has a large divergence, and so the output is spread in energy. The fact that such a large fraction of the input beam is unwound is due to the stability of the unwinding orbits.[3] The reason for the large spread in parallel energy of the input beam is not yet understood.

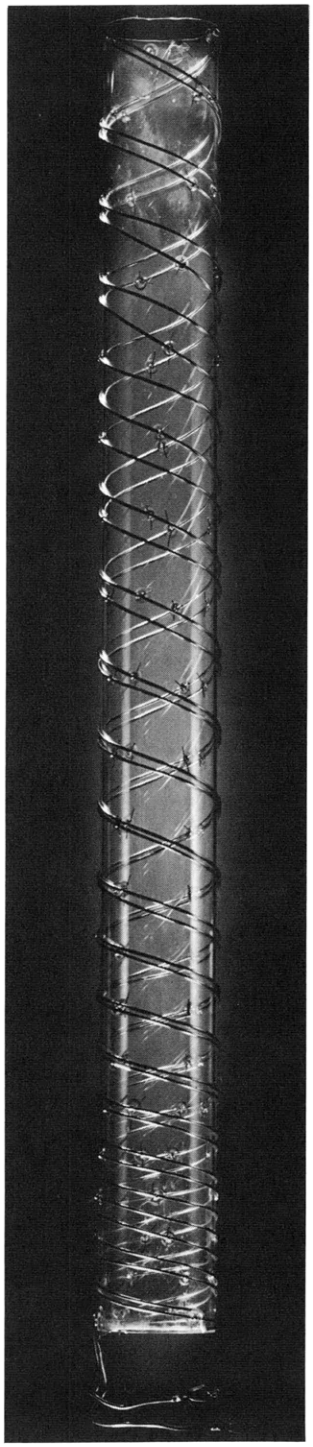

Fig. XIII-3. Perturbation field coil "Corkscrew."

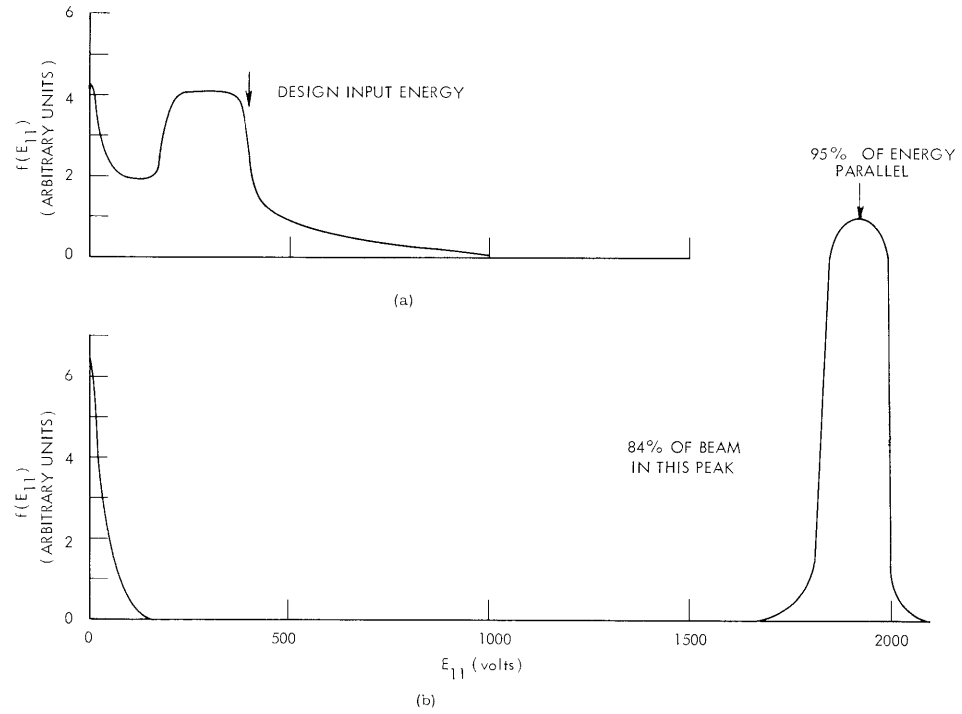

Fig. XIII-4. (a) Parallel energy distribution of the beam at the entrance to the corkscrew.
(b) Parallel energy distribution of the beam at the exit of the corkscrew.

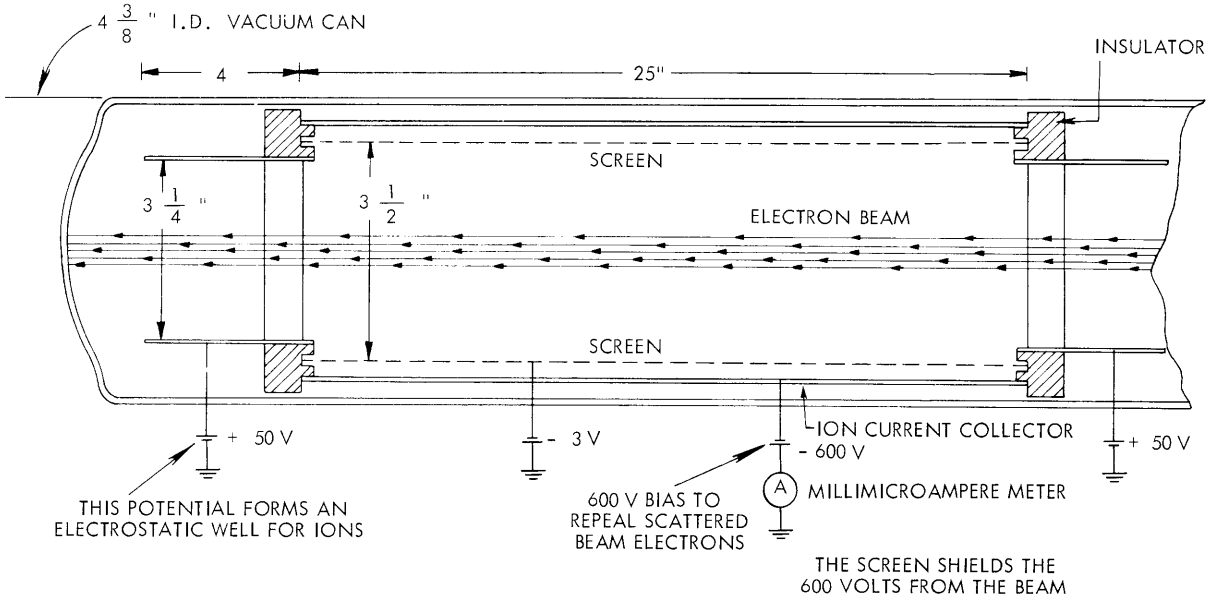

Fig. XIII-5. Ion collector.

With the aid of fluorescent screens and grids which could be rotated into the beam path, we ascertained that the beam was, in fact, closing on itself. In order to measure the number of transits around the device, we employed the ion collector[4] shown in Fig. XIII-5. The ion current collected is proportional to the electron current and the background gas pressure. By bending the beam into the wall after it passes through the collector, we measure I_1, the ion current for one transit. Then I_N is measured for the closed circulating beam. The average number of transits, N, is the ratio of the measured currents, I_N/I_1. By varying the vertical field on the U-bends to obtain the "best" beam closure, N was maximized at approximately 15.

If all the loss was due solely to a directed drift, then $N = v_{\perp o}/\langle \Delta v_\perp \rangle$, and if the loss was due solely to random steps, then $N = v_{\perp o}^2/\langle \Delta v_\perp^2 \rangle$. In reality we have a combination of both; however, we can take the two extreme cases and place upper bounds on $\langle \Delta v_\perp \rangle$ and $\langle \Delta v_\perp^2 \rangle^{1/2}$ as follows. $v_{\perp o}$ is proportional to the radius to the gun snout, 1.4 cm (see Fig. XIII-2), and v_o is proportional to $r_{b_o} = 2.1$ cm. Also, we assume that the guiding center stays on the axis.

$$\frac{\langle \Delta v_\perp \rangle}{v_o} < \frac{v_{\perp o}}{N v_o} = \frac{1.4}{15 \times 2.13} = .04$$

$$\frac{\langle \Delta v_\perp^2 \rangle^{1/2}}{v_o} < \frac{v_{\perp o}}{N^{1/2} v_o} = \frac{1.4}{15^{1/2} \times 2.13} = .17$$

A theoretical description is being worked out simultaneously with the experimental work and runs as follows. Let f be a vector whose components f_i equal the number of electrons with normalized magnetic moment $s = v_\perp^2/v_o^2$ between $s_i \leq s < s_{i+1}$. Then

$$\frac{df(s,t)}{dt} = Of(s, t-t') - Lf(s, t-t') + S(s,t),$$

where t' is the transit time,

$$f = \begin{bmatrix} f_1 \\ f_2 \\ \vdots \\ f_n \end{bmatrix} = \text{distribution function} \qquad S = \begin{bmatrix} S_1 \\ S_2 \\ \vdots \\ S_n \end{bmatrix} = \text{source}$$

$$O = \begin{bmatrix} O_{11} & O_{12} & \cdots & O_{1N} \\ O_{21} & & & \\ \vdots & & & \\ O_{N1} & & & O_{NN} \end{bmatrix} = \text{scattering in matrix}$$

$$L = \begin{bmatrix} L_1 & & & 0 \\ & L_2 & & \\ & & L_3 & \\ & & & \ddots \\ 0 & & & L_N \end{bmatrix} = \text{scattering out matrix}$$

where

O_{ij} = probability that an electron in the j^{th}, s interval when it enters the "corkscrew" perturbation field will make a transition to the i^{th}, s interval divided by the time that the electron took to make one transit of the torus.

O_{ii} is set to zero, since this transition does not contribute to df/dt.

L_i = probability that an electron in the i^{th}, s interval will make a transition out of the i^{th}, s interval divided by its transit time.

For the steady state,

$$df/dt = 0$$

$$f = -(O-L)^{-1}S.$$

The elements of the O and L matrix are obtained by numerically integrating the equation of motion for a given input s and many phase angles θ, which gives an s at the output for each θ at the input. From these computations the probabilities can be constructed, the O-L matrix can be formed, and the inverse obtained on the computer. This gives the steady-state distribution.

We have divided s space into 9 intervals plus the "loss cone" where s(loss) = 0.44 (see Fig. XIII-6) and where the guiding center has been assumed to remain on the axis. The results are

$$N = \frac{\sum_{i=1}^{9} f_i \Delta s_i}{\sum_{i=1}^{9} s_i \Delta s_i} = 6.4 \text{ transits.}$$

It is quite likely that the discrepancy between measured and computed values results from a slow downward drift of the beam when the circulating current is experimentally maximized. This would move the particle guiding centers away from the injection snout even as they scattered in s and so reduce the effective size of the velocity-space loss cone.

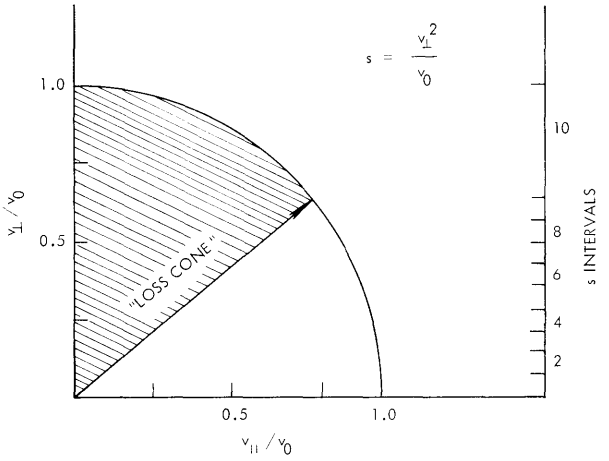

Fig. XIII-6. Loss cone in velocity.

The number of transits obtained experimentally and computationally are preliminary, and work is in progress to improve the techniques; however, the number of transits is large enough to be used for measurements of diffusion produced by added perturbating fields as originally planned.

R. W. Moir, L. M. Lidsky

References

1. Quarterly Progress Report No. 77, Research Laboratory of Electronics, M.I.T., April 15, 1965, pp. 164-167; Quarterly Progress Report No. 78, July 15, 1965, pp. 126-127; Quarterly Progress Report No. 79, October 15, 1965, pp. 131-132.
2. R. C. Wingerson, T. H. Dupree, and D. J. Rose, Phys. Fluids 7, 1475 (1964).
3. L. M. Lidsky, Phys. Fluids 7, 1484 (1964).
4. A. P. Slabospitskii and V. D. Fedorchenko, International Atomic Energy Conference on Plasma Physics and Controlled Nuclear Fusion Research, Culham, United Kingdom, 6-10 September 1965, Paper CTO/105.

C. NONADIABATIC SCATTERING IN MAGNETIC FIELDS

1. Measurements of Particle Escape from a Corkscrew Magnetic Trap

Figure XIII-7 shows the experimental apparatus that is being used to investigate the trapping and loss of particles in a "corkscrew"[1] nonadiabatic magnetic field. A 1600-volt

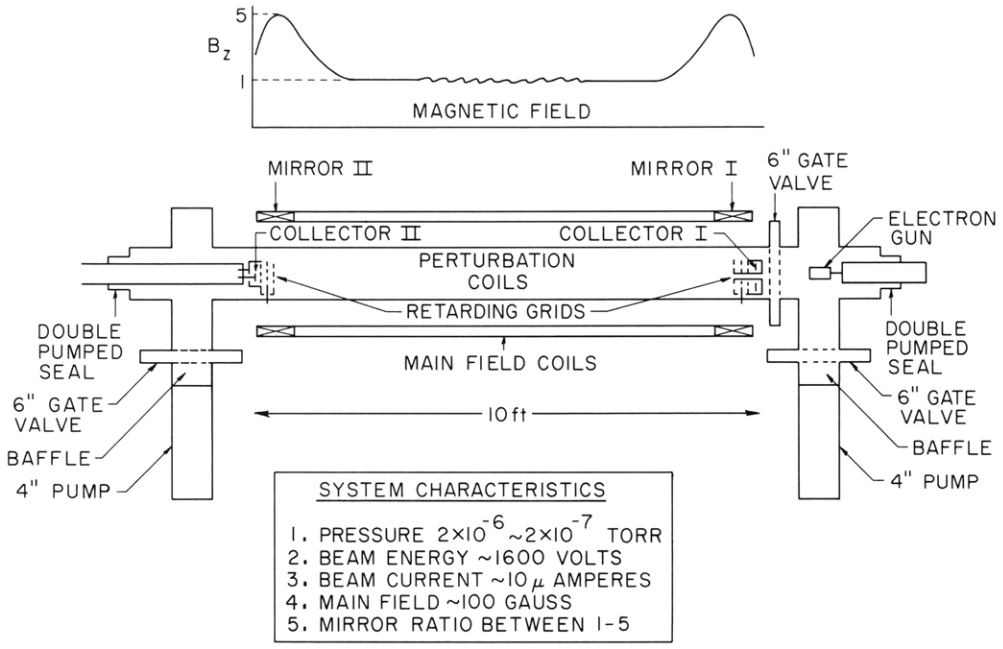

Fig. XIII-7. Nonadiabatic trapping experiment.

5-10 μamp electron beam was injected parallel to the axis of the system through a tube piercing the center of Collector I which was located just outside Mirror I. Mirror I was adjusted to produce a 1:1 mirror ratio, and Mirror II was set at 5:1. With no corkscrew current, the beam struck Collector II where its energy spectrum was measured by the retarding-potential method. When the corkscrew current exceeded 25 amps, the beam was given sufficient transverse energy to be reflected by Mirror II and was collected by Collector I. Mirror II was then set equal to Mirror I so that the beam was trapped. Under these conditions 70% of the beam current escaped through Mirror II and practically none through Mirror I. The rest presumably escaped radially or was stopped by the detector screens. An increase of current to an unshielded annular detector was noted, but no quantitative measurements were made because secondary electrons and ions could not be

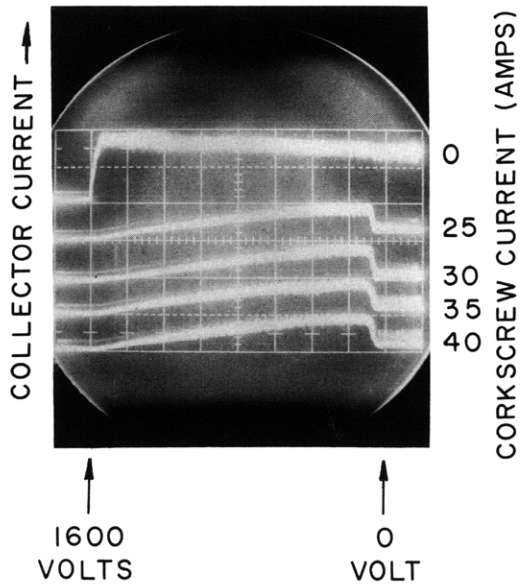

Fig. XIII-8. Escaping particle current as a function of retarding potential.

separated from the injected particles.

Figure XIII-8 shows the energy analysis made at Collector II for 5 values of the corkscrew current. In this figure the particles are distributed from 1600 volts (the total beam energy) to nearly zero. This is due to the position of Collector I in the mirror's throat. Particles that are scattered into the loss cone in the uniform central region have parallel energies ranging from 1600 volts to 1280 volts, the minimum parallel energy necessary to penetrate the mirror. As the 1280-volt particles move farther into the mirror from the central field region, conservation of magnetic moment converts parallel into perpendicular energy. Just at the mirror neck these particles have zero parallel energy, while the 1600-volt particles, which have zero magnetic moment, still possess all of their parallel energy.

The dip on the right in Fig. XIII-8 is due to the analyzing screen swinging positive and collecting the beam. This point locates the zero retarding voltage. The first trace, which is for the unperturbed beam, indicates the 1600-volt point. A similar energy analysis taken with the detector retracted to a 100-gauss region outside the mirror accurately reproduces the distribution of particles in the loss cone within the trap at any instant. A derivative of this curve, which is proportional to the parallel energy distribution of the particles, is shown in Fig. XIII-9 superimposed on an energy-space diagram. It is apparent that the peak of this distribution lies well inside the edge of the loss cone. This indicates the existence of a strong preferential scattering as opposed to a diffusive loss mechanism.

The decay of the trapped particles was observed for pulsed injected beams. Figure XIII-10 shows a typical result. The lower trace is for zero corkscrew current and shows that the rise time of the detection circuit is less than 0.5 μsec. The upper curve is for a corkscrew current of 38.5 amps. The signal is constant at its equilibrium level for approximately 3 transit times after the beam is cut off. This indicates that the dominant loss of particles is associated with the second and subsequent forward transits of the perturbation. The decay is exponential to the limiting detector sensitivity and has a time constant of 1.49 μsec.

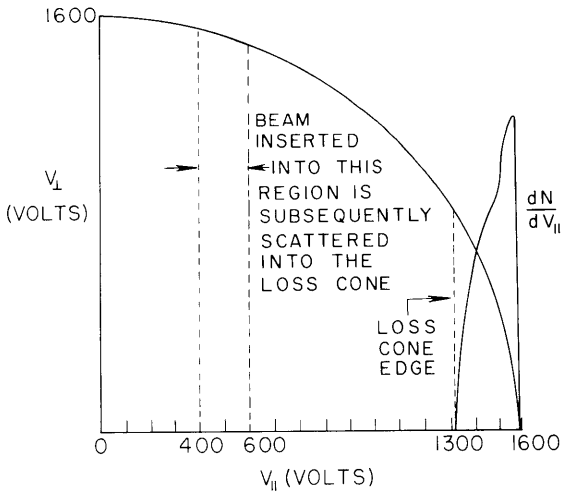

Fig. XIII-9. Loss-cone particle distribution as a function of their parallel energy.

A series of decay curves for varying corkscrew currents were obtained, and the decay time as a function of this

current is shown in Fig. XIII-11. In each case the decay was exponential to the limit of detector sensitivity. Because of this limit on sensitivity (~5% of the equilibrium signal),

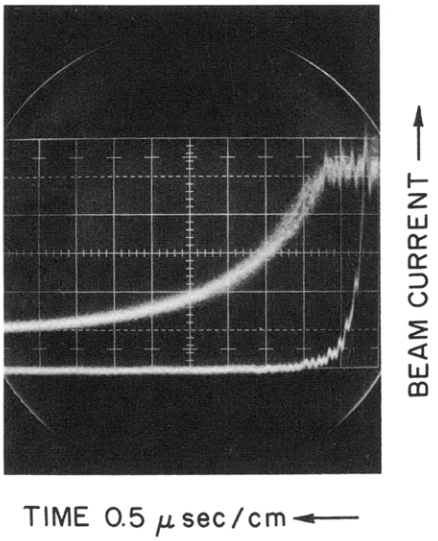

Fig. XIII-10. Upper trace: Trapped particle decay. Lower trace: Untrapped beam.

the existence of a group of long-lived particles is not ruled out. For example, a group of particles trapped in a region of velocity space where their lifetime against scattering was 15 μsec would be undetected unless their density exceeded 50% that of the fast-decaying group. We are now at work on this problem. Figure XIII-11 does indicate that the maximum lifetime occurs at the design current of the corkscrew.

For helical resonant trapping, the product of the current and the cosine of the design phase angle is a constant. At lower currents the particle must follow closer to the position of maximum radial field to follow the resonant orbit. Such orbits have been shown to be less stable,[2] and the particle will experience less windup. On the third pass these particles having more $v_{||}$ will be locally resonant nearer to the center of the corkscrew where the perturbation is strongest and will be lost rapidly. For currents higher than the design current, the particle sees a higher perturbation field and is lost rapidly because the scattering is stronger.

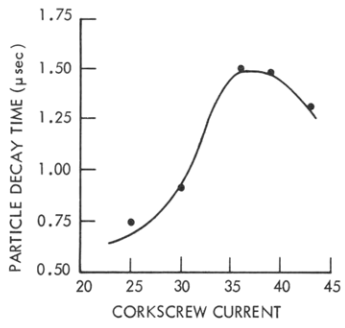

Fig. XIII-11. Lifetime as a function of corkscrew current.

The rapid initial loss of particles and the preferential forward scattering reported above were not predicted by the previously existing theories of nonadiabatic scattering.[3,4] These experiments have motivated a new approach to

the description of this scattering which is outlined below.

The experiments described here were performed with a seven-turn corkscrew. In order to obtain a better test of existing theoretical analyses, a highly tuned fifteen-turn corkscrew was built and is being tested. This "Mark II corkscrew" has a screened radial particle detector which should yield more accurate particle accountability. Also, a scintillator-photomultiplier electron detection system was tested. Preliminary results show that we might be able to increase the sensitivity of the lifetime measurements enough to allow a conclusive check on the existence of a substantial long-lived group.

2. Validity of Stochastic Descriptions of Nonadiabatic Motion

The system under consideration can be idealized as in Fig. XIII-12. In a particular case the fields in the magnetic-moment nonconserving region might be due either to a

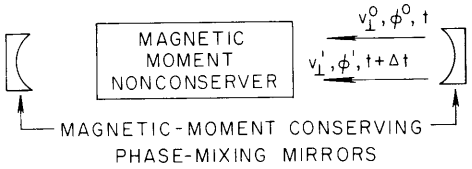

Fig. XIII-12. Idealization of a non-adiabatic trap.

plasma wave or to external current windings and, in any case, they will be assumed to be known functions of space and time. Thus, we shall consider purely deterministic systems. The conditional probability per unit $v_\perp$ and ϕ that for given $v_\perp^o$ and ϕ^o one will observe $v_\perp'$ and ϕ' between $v_\perp'$ and $v_\perp' + \Delta v_\perp'$ and ϕ' and $\phi' + d\phi'$ after a transit time Δt is

$$P_2\left(v_\perp^o \phi^o / v_\perp' \phi' \Delta t\right) = \delta\left(v_\perp' - v_\perp^s\right) \delta\left(\phi' - \phi^s\right) \tag{1}$$

where

$$v_\perp^s = v^s\left(v_\perp^o, \phi^o\right)$$

$$\phi^s = \phi^s\left(v_\perp^o, \phi^o\right)$$

are solutions of the equations of motion. But ϕ varies between zero and 2π many times during the particle's orbit, so that ϕ' and ϕ^o appear to be uncorrelated. Symbolically, we can write the conditional probability as

$$P_2(\phi^o / \phi' \Delta t) \doteq \frac{1}{2\pi}. \tag{2}$$

In a magnetic trap we are mainly interested in describing the statistical behavior of a particle's magnetic moment and so concern ourselves with $v_\perp$. To simplify the problem

of solving N orbit equations for N particles, it is tempting to employ the pseudorandom character of the phase ϕ.

If we allow some uncertainty in ϕ^o, the delta function in Eq. 1 is broadened to the extent of this uncertainty. Furthermore, one might hope that in the weak-field limit the change in $v_\perp$ per transit would be small. If we make this assumption, we can state that the conditional probability (1) is a sharply peaked function around

$$v_\perp' = v_\perp^o + \Delta v_\perp^o\left(\phi^o, v_\perp^o\right), \tag{3}$$

where

$$\Delta v_\perp^o \ll v_\perp^o.$$

Then, if we ignore the initial phase dependence of the small quantity $\Delta v_\perp^o$, the conditional probability (1) becomes

$$P_2\left(v_\perp^o\phi^o/v_\perp'\phi'\Delta t\right) = P_2\left(v_\perp^o/v_\perp'\Delta t\right)\, P_2\left(\phi^o/\phi'\Delta t\right), \tag{4}$$

where the velocity conditional probability is peaked around $v_\perp^o$. If the initial phase dependence of $\Delta v_\perp$ is not ignored, the separation in (4) is not valid. We shall show that the results of the existing stochastic theories depend on this assumption and consequently will fail if the assumption proves untenable.

The conditional probability in (4) can be used to generate a Fokker-Planck equation in the usual way with the exception that higher order terms are not dropped because they are proportional to high powers of the elemental time steps. They are dropped solely because the small-field assumption ensures that they are small. The result is

$$\Delta f = 2\,\frac{\partial}{\partial s}\left\{-\sqrt{s}\,\frac{\overline{\Delta v_\perp}}{v} + \frac{\sqrt{s}}{2}\,\frac{\partial}{\partial s}\left(\frac{\overline{\Delta v_\perp^2}}{v^2}\right)\right\} f + 2\,\frac{\partial}{\partial s}\left(s\,\frac{\overline{\Delta v_\perp^2}}{v^2}\right)\frac{\partial}{\partial s} f, \tag{5}$$

where

$$s = v_\perp^2/v^2$$

$$\overline{\Delta v_\perp^n} = \int_0^{2\pi} d\phi' \int_0^v dv_\perp'\, \Delta v_\perp^n P_2\left(v_\perp^o\phi^o/v_\perp'\phi'\Delta t\right). \tag{6}$$

If we make the pseudorandom approximation, we may replace the integration over ϕ' by integration over ϕ^o and, by using Eq. 4, find

$$\overline{\Delta v_\perp^n} = \int_0^{2\pi} d\phi^o\, \Delta v_\perp^n\Big|_{v_\perp^o} P_2(\phi^o/\phi'\Delta t) \tag{7}$$

and by using (2) get

$$\overline{\Delta v_\perp^n} = \int_0^{2\pi} \frac{d\phi^o}{2\pi} \Delta v_\perp^n \Big|_{v_\perp^o} . \tag{8}$$

This is the starting point of the previous stochastic theories.[4] We have shown that it is based on the assumption that the probability of the transition $v_\perp^o \rightarrow v_\perp'$ is independent of ϕ^o. This assumption is only true in the limit of zero perturbation. Numerical analysis will show that it does not apply in the case of the corkscrew magnetic trap.

The consequence of the usual assumption (Eq. 8) is that the dynamical friction term in Eq. 5 is of second order and is in fact cancelled by the second term in braces. We are left with

$$\Delta f = \frac{\partial}{\partial s} 2s \left(\frac{\overline{\Delta v_\perp^2}}{v^2} \right) \frac{\partial f}{\partial s} \tag{9}$$

which predicts only currents proportional to the second power of the small field quantities. In other words, Eq. 9 predicts a current resulting from the dependence of the diffusion coefficient on s, but it cannot account for a current caused by a preferred direction of scattering.

If $P_2\left(v_\perp^o \phi^o / v_\perp \phi \Delta t\right)$ is not split up as indicated above, we might still assume that it is peaked around $v_\perp^o$ on the basis of perturbation theory. In this case, however, Eq. 8 should be written

$$\overline{\Delta v_\perp^n} = \int_0^{2\pi} \frac{d\phi^o}{2\pi} \Delta v_\perp^n \Big|_{v_o} F(\phi^o), \tag{10}$$

where $F(\phi^o)$ is an unknown function containing the previously neglected phase dependence of the conditional probability. Now the dynamical friction term in the Fokker-Planck equation is of first order in the small-field quantities. This could lead to a much larger directional scattering than was previously suspected. Such rapid loss has been observed experimentally and is consistent with numerical analysis of particle motions.

3. Digital-Statistical Description of Nonadiabatic Scattering

The equations describing the motion of a particle in a nonadiabatic magnetic field are[1]

$$\frac{dv_\perp}{dz} = \omega_\perp(r, z) \cos \chi \tag{11}$$

$$\frac{dx}{dz} = \frac{\omega_o}{v} - \frac{2\pi}{p(z)}, \tag{12}$$

where $\omega_\perp$ and ω_o are $qB_\perp/m$ and qB_o/m, respectively, and p is the pitch of the perturbation field $B_\perp$. Most of the interaction between a particle beam and the nonadiabatic field in a magnetic trap take place near the axis. Then Eqs. 11 and 12 can be simplified by neglecting the radial dependence of $\omega_\perp$. Employing this assumption and the normalizations of Lidsky,[2] we obtain a simplified set of equations which closely describes the motion of a particle in a corkscrew

$$\frac{dv}{dx} = \alpha \sin 2x \frac{\cos \chi}{\cos \chi_o} \tag{13}$$

$$\frac{d\chi}{dx} = \Lambda\left(\frac{1}{\sqrt{1 - v^2}} - \frac{1}{p(x)}\right). \tag{14}$$

The parameters are defined as follows:

α^2 = final magnetic moment after one transit in the equilibrium orbit

p = corkscrew pitch normalized to its initial value p_o

χ = a phase angle between the particle's position and the field maximum

χ_o = phase angle in equilibrium orbit

$\Lambda = 4L/p_o$ normalized corkscrew length

$x = \pi z/2L$.

These equations were solved numerically to determine the change in a particle's magnetic moment as a function of the initial phase. Typical results are shown in Fig. XIII-13. This is a plot of the relative field-particle phase χ as a function of position along the corkscrew for a particle of initial magnetic moment 0.40 and various initial phases. The insert shows the final magnetic moment as a function of initial phase. The insert also shows that particles increase their magnetic moments over only 17% of the possible initial phases. In other words, a particle with random initial phase has an 83% probability of decreasing its magnetic moment. This is a startling conclusion that clearly invalidates the stochastic theory already referred to. The physical reason for this preferential downward scattering can be seen by examining the phase curves above the insert in Fig. XIII-13. Upon entrance to the corkscrew, a particle with 40% initial windup is rotating faster than the field in the frame moving with the particle's axial velocity. Thus the phase is initially increasing as shown. Since the perturbing field pitch is decreasing along the axis, there is some point where the field and particle will rotate with the same angular velocity. This resonance condition is expressed analytically by

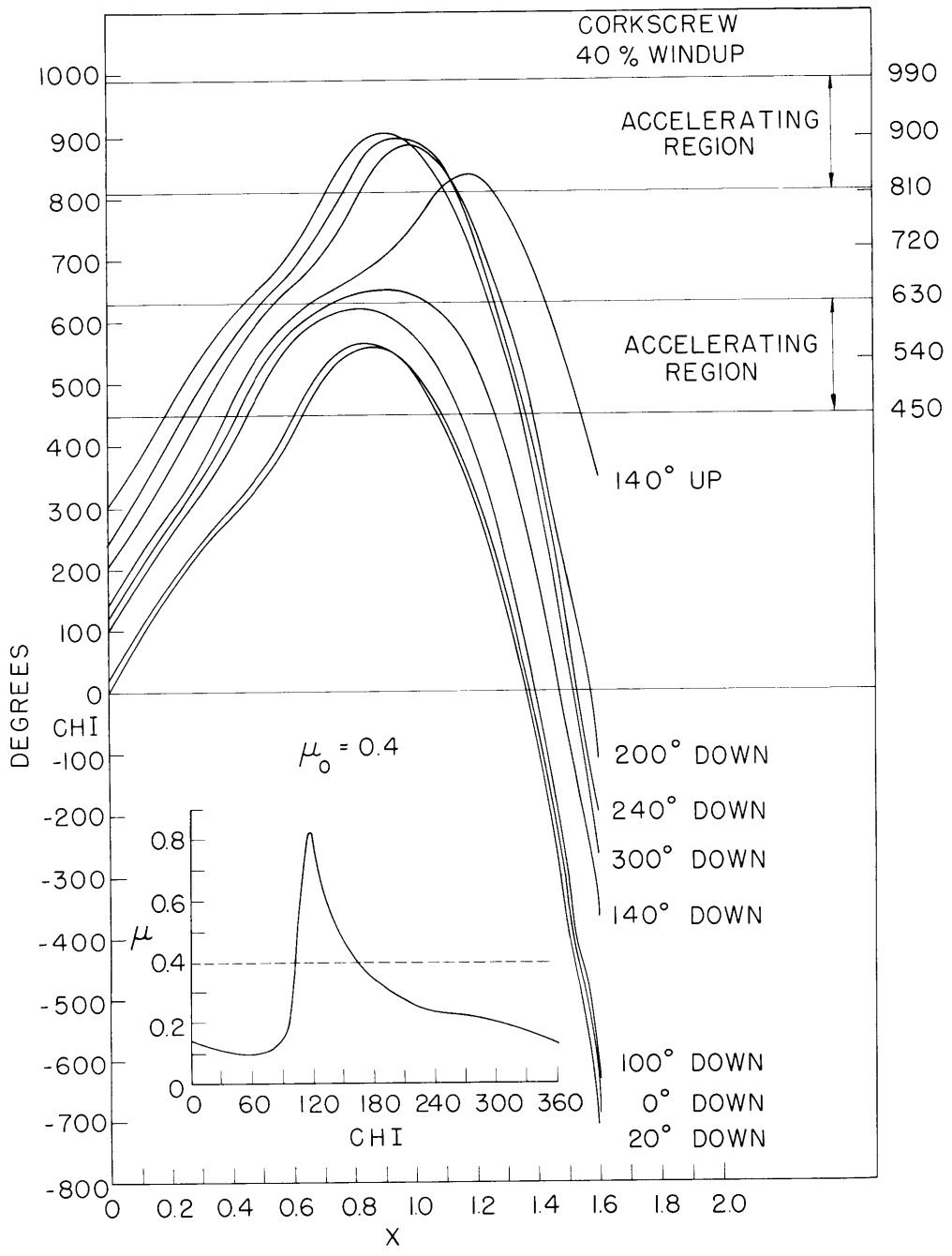

Fig. XIII-13. Computer analysis of trapped-particle motion.

$$\frac{d\chi}{dx} = 0 \tag{15}$$

These zero slope points are shown in Fig. XIII-13, and we shall refer to them as turnover points.

Referring to Eq. 13 one notes that the direction of the change in the perpendicular velocity (and consequently in the magnetic moment) is determined by the relative field-particle phase χ. In Fig. XIII-13 we have indicated two phase quadrants in which the particle loses magnetic moment as "acceleration regions" since a particle losing magnetic moment is accelerated along the field. If a particle has a turnover point in such a region, it experiences a resonant accelerating interaction. Figure XIII-13 shows that most of the curves have turnovers in the accelerating region. The curve for 140° initial phase which starts to turn over in the middle of the deceleration region is pushed upward into the next accelerating quadrant.

The physical basis for preferential acceleration can be seen by examination of the necessary condition for turnaround. From (12) we get the turnaround condition

$$\frac{d^2\chi}{dz^2} = \frac{2\pi}{p^2}\frac{dp}{dz} + \frac{\omega_o}{\left(v^2 - v_\perp^2\right)^{3/2}} v_\perp \frac{dv_\perp}{dz} < 0 \tag{16}$$

Employing the resonance condition, we obtain

$$\frac{2\pi}{p} = \frac{\omega_z}{\left(v^2 - v_\perp^2\right)^{1/2}}, \tag{17}$$

and by using Eq. 11 this reduces to

$$\frac{d^2\chi}{dz^2} = \left[\frac{2\pi}{p}\right]^2 \left[\frac{v_\perp \omega_\perp}{\omega_o^2}\right][\cos\chi - \cos\chi_o]. \tag{18}$$

This shows that for the corkscrew there is a forbidden region in phase where turnaround is impossible. This forbidden region covers the range of phase where the particle sees the maximum decelerating force. Thus, since the particle cannot come into resonance in the most effective part of the decelerating region, its average step will be an acceleration.

When we look at the physics of this effect, we see that it is more general than the derivation above might indicate. Consider Eq. 11 which has general validity. Given a particle that is rotating faster than the field, this equation tells us that $v_\perp$ fluctuates as χ increases; however, it is the particle's z velocity which causes χ to change. The

faster v_z, the slower χ fluctuates. Alternatively, the slower $v_\perp$, the slower χ fluctuates. Thus decelerating regions which decrease v_z have, on the average, more fluctuations than equivalent accelerating regions. The net result is a preferential downward scattering in resonant systems with pitch-length decrease in the direction of particle motion. Another way of stating this is that χ tries to become stationary by decreasing $v_\perp$. If it finds itself in a decelerating quadrant, it tends to move onward into the next favorable quadrant. This effect is shown in the 140° initial phase case in Fig. XIII-13.

We have also performed calculations on a Whistler model field. This is a helical field with a linear phase variation along its axis. Although this calculation was not scaled to any physical system supporting real waves, the effect noted above did appear. We feel that with proper scaling Eqs. 11 and 12 should apply to the ionosphere. The necessary calculations to check this scaling are being performed.

We have tried to indicate just how perturbation theory fails in the presence of preferential scattering. Figures XIII-14 and XIII-15 show the mean step and mean-square step in $v_\perp^2/v^2$ obtained from our orbit calculations and from perturbation theory.[3] We have indicated that preferential scattering will generate a current term proportional to the first power of the field variable and also modify the second-order diffusion coefficients. The magnitude of the discrepancy depends upon the relative width of the forbidden zone, and is a complicated function of the details of the resonant-field perturbation. The discrepancy becomes more important as the size of the normalized velocity steps decreases because the confinement time is proportional to N^{-1} for currentlike and to N^{-2} for diffusivelike losses, where N is approximately $v^o/\Delta v^o$.

The peak at $v_\perp^2/v^2 = 0.35$ in Fig. XIII-13 is a case in point. This initial magnetic moment displays the same behavior as that shown in the insert in Fig. XIII-13 which is for $v_\perp^2/v^2 = 0.40$. The difference is that the 0.35 case has a narrow range of initial phases that place the particle in the design orbit somewhere in the corkscrew. The particles with their initial phases make very large steps upward in magnetic moment and bias the mean-step upward. A particle with random initial phase will probably still make a step downward. Thus, in this case, the Fokker-Planck equation with its average coefficient $\overline{\Delta s}$ is not truly descriptive of the situation. Thus, the results of Section I call into question the utility of the Fokker-Planck equation in describing the solution of the distribution function in systems of physical interest even if asymmetric scattering is correctly taken into account. Particles may fall into near-resonant orbits and suffer selectively large perturbations. This behavior violates the essential assumption that the distribution function changes slowly in the time scale describing individual particle motion.

To describe the evolution of a particle distribution in a nonadiabatic trap, we have developed a numerical-statistical analysis which we hope combines the economy of a statistical approach with the accuracy of digital computation. Our basic postulate is that

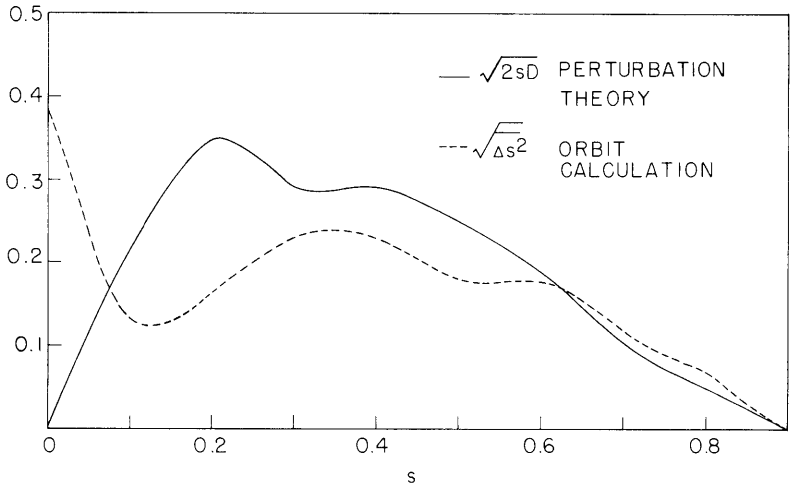

Fig. XIII-14. Mean change in magnetic moment per transit.

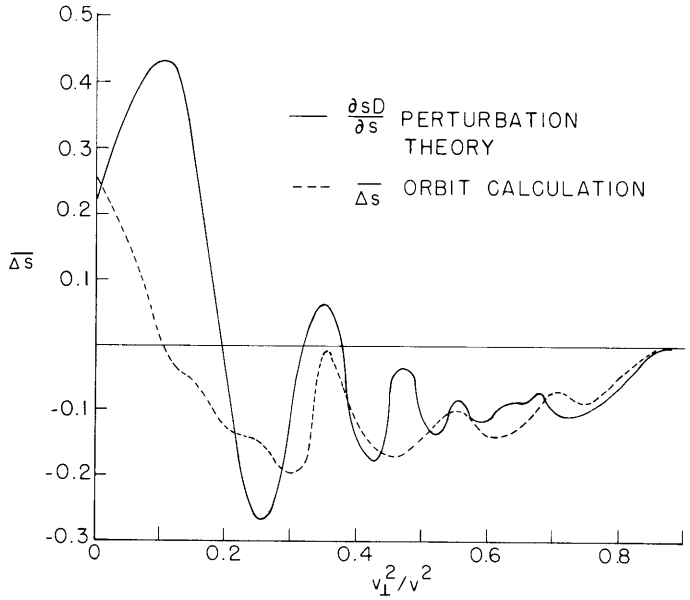

Fig. XIII-15. RMS change in magnetic moment per transit.

our system can be described by a scattering matrix, each term of which gives the probability of a particle's transition from a "state" of magnetic moment s_1 to a "state" s_2. Each term in this matrix is obtained from numerical orbit calculations and is given by

$$P_{ij} = \frac{\Delta\phi_{ij}}{2\pi},$$

where $\Delta\phi_{ij}$ is the range of initial phases for which a particle with a magnetic moment within a small range of s_j will scatter into a small range of s in a suitably normalized time interval. The time evolution of the distribution is given by

$$\Delta s_i = S + P_{ij} D s_j - s_i,$$

where Δs_i is the change in density of forward-streaming particles in magnetic moment interval i, S_i is the external source of such particles, P_{ij} is the matrix representing scatter from group j to group i, and D_j is the operator describing the mirror losses and variable transit time delays. Thus we are able to compute both the transient and steady-state behavior of the system and, in particular, to compute the particle currents through either mirror. These results will be directly comparable with the experimental measurements described in Section I.

J. F. Clarke, L. M. Lidsky

References

1. R. C. Wingerson, Phys. Rev. Letters 6, 446 (1961).
2. L. M. Lidsky, Phys. Fluids 7, 1484 (1964).
3. R. C. Wingerson and T. H. Dupree, Phys. Fluids 7, 1475 (1964).
4. J. F. Clarke, S.M. Thesis, Department of Physics, M.I.T., 1964.